Journal of Sound and Vibration 473 (2020) 115229

Contents lists available at ScienceDirect

Journal of Sound and Vibration

journal homepage: www.elsevier.com/locate/jsvi

Special Issue at the occasion of the ISMA2018 International Noise and Vibration Conference

Numerical modeling of a flexural displacement-converter mechanism to excite a flat acoustic source driven by piezoelectric stack actuators

F. Tajdari [a,*], A.P. Berkhoff [a,b], A. de Boer [a]

[a] University of Twente, Faculty of Engineering Technology, Drienerlolaan 5, 7500 AE, Enschede, the Netherlands
[b] TNO Technical Sciences, Acoustics and Sonar, Oude Waalsdorperweg 63, 2597AK, Den Haag, the Netherlands

ARTICLE INFO

Article history:
Received 7 March 2019
Revised 15 January 2020
Accepted 30 January 2020
Available online 5 February 2020
Handling Editor I. Trendafilova

Keywords:
Thin acoustic source
Low frequency
Piezoelectric stack actuators
Flexural mechanism
Finite element

ABSTRACT

This paper studies an acoustic source with a relatively small thickness and a high bending stiffness. The acoustic source operates in the low frequency, quasi-static regime. The focus of the current study is on the actuation part in order to design an appropriate excitation mechanism. A flexural mechanism is modeled in combination with a piezoelectric actuator to convert an in-plane displacement of the actuator to the out-of-plane direction. First, an optimization simulation is used to determine the size of the required piezoelectric actuator. An equivalent electrical circuit of the lumped acoustic source is used for the optimization. A coupled 3D numerical finite element (FE) analysis is carried out using COMSOL Multiphysics software package. The fully-coupled analysis combines the suggested flexural mechanism, the piezoelectric stack actuator, and the thin acoustic source. Finally, the sound pressure field that is generated by the thin acoustic source is investigated and compared using both the finite element analysis and the lumped model.

© 2020 Elsevier Ltd. All rights reserved.

1. Introduction

Stiff and light sandwich structures with high bending stiffness can be used to obtain piston-like motion of the radiating surface of acoustic sources [1]. Light-weight sandwich structures have been used in active control techniques for a reduction in the transmitted sound [2,3]. Sandwich structures have been studied widely in vibro-acoustic applications in recent years [4–6]. The vibro-acoustics characteristics of sandwich structures with honeycomb cores are examined in Ref. [7]. A reduced thickness can be achieved by perforating the interior face of the sandwich plate in order to be able to use the air volume inside the honeycomb cells. Perforation of thin structures in some applications leads to a reduction in the radiated sound [8]. The radiation efficiency of the perforated panels is examined in Refs. [8,9].

Only acoustic sources that are sufficiently larger than the wavelength are able to emit sound in the form of propagating waves [10]. In some applications, the limited build space restricts the size of acoustic sources. Thin acoustic sources with a thickness that is relatively smaller than the characteristic length of the surface can be useful in applications with limited build space, especially at low frequencies. They can be employed in active sound absorption, active noise control, flat loudspeakers,

* Corresponding author.
E-mail addresses: f.tajdari@utwente.nl (F. Tajdari), a.p.berkhoff@utwente.nl (A.P. Berkhoff), a.deboer@utwente.nl (A. de Boer).

https://doi.org/10.1016/j.jsv.2020.115229
0022-460X/© 2020 Elsevier Ltd. All rights reserved.

and in ducts [11]. However, the efficiency of the thin sources is restricted by the size of the enclosure [12]. Both limited build space and low radiation efficiency contribute to the complexity of the design of thin acoustic sources at low frequencies.

A few thin acoustic sources with a thin enclosure thickness, and a large enclosure's surface area have been designed and studied recently [13,14]. A double-layer sandwich panel is made of two face sheets that are separated from each other by an air aperture, and is investigated in Ref. [15] to be used in a thin acoustic source. Although flat acoustic sources are investigated in a few studies, there seem to be not so many currently used thin sandwich acoustic sources in practice that fulfill all the following characteristics:

- Structures that are exclusively designed to generate good quality sound at low frequencies rather than eliminating sound transmission,
- Acoustic sources that are thin and light-weight using sandwich structures,
- Acoustic sources that are energy-efficient with minimum energy loss, especially at low frequencies.

One available thin sandwich acoustic source that focuses on the generation of sound at low frequencies is described by Berkhoff [13]. However, due to the use of voice coil actuators, the suggested acoustic source in Ref. [13] dissipates a large portion of the input electrical energy and is not considered energy-efficient.

In the current research, the thin acoustic source that is introduced in Refs. [13,14] is studied to achieve a uniform, rigid body motion. Various actuators including voice coil actuators [13] and piezoelectric patch actuators [14] are studied as the excitation units of this thin acoustic source. The use of voice coil actuators as the driver of the suggested thin acoustic source is examined in Ref. [14]. However, as mentioned earlier, voice coil actuators dissipate a large portion of the input electric power due to Joule heating of the coil. In particular, in the low frequency applications, the majority of the electric power that is delivered by the connected electrical amplifier to the driver, is dissipated in the voice coil device. Therefore, a small portion of the input electric power is converted to mechanical power to excite the thin acoustic source. As a result, a disadvantage of the acoustic source in Refs. [13,14] is that extra input electric power is needed to feed the voice coil driver. Consequently, using a voice coil actuator leads to an inefficient thin acoustic source system. An inefficient acoustic source consumes extra input electric energy, which causes energy loss and high energy expenses. A piezoelectric stack actuator may be used as an alternative driver in the design of the thin source. Piezoelectric devices are energy efficient structures due to their capacitive nature. The power loss in a piezoelectric actuator is negligible in comparison with the stored power in the capacitive part. Therefore, piezoelectric actuators are efficient choices to ensure an energy efficient operation of the thin acoustic source. The possibility of using piezoelectric stack actuators has been investigated when a lumped model of the thin acoustic source is used [10].

The main contribution of the present paper is to obtain an optimum actuation unit for the thin sandwich acoustic source that can lead to an energy-efficient light-weight source with maximum acoustical radiation power, especially when operating at low frequencies (below 1000 Hz). The optimum actuation unit has to be designed in such a way that it can be employed in the limited build space of the thin acoustic source. Optimization methods have been widely used in source localization and microphone arrays applications [16–18], and in active treatments of acoustic sources [19]. In the current paper, an optimization method is employed to obtain a maximum acoustical radiation power of the thin sandwich acoustic source. The possibility of using piezoelectric stack actuators in the design of the thin acoustic source is investigated. As a result of the optimization study, however, it is concluded that due to limited space, piezoelectric stack actuators cannot directly be used as the excitation part of the thin acoustic source. Therefore, the design of a displacement-converter mechanism is crucial. With the aid of a displacement-converter mechanism, piezoelectric stack actuators can be used while their displacement in one direction is converted to a displacement in a desired direction. The investigated actuation unit is mainly a displacement-converter mechanism. Therefore, an amplification in the amplitude of the input motion is not of high importance in the present study.

Flexures are elastically deforming parts that provide a precise range of motion in the desired degrees of freedom. The produced motion is predictable and repeatable [20]. These compliant mechanisms have a relatively high stiffness in the constrained directions [21]. Due to the fact that flexures are both frictionless and maintenance-free [21], they can be used in the design of the required motion-converter mechanism in the current research. The required motion-converter has to fulfill the following conditions:

- The required motion-converter can convert the direction of an initial motion to an out-of-plane final motion that is perpendicular to the initial motion,
- The required motion-converter has an operating frequency in the low frequency range below 1000 Hz.
- The required motion-converter can deliver the needed stroke and force to the thin acoustic source,
- The required motion-converter is thin in the direction of the final motion, so that it can be employed in the limited build space of the thin acoustic source.

Several flexural designs are already designed and manufactured. Commercial designs are widely used in industry [22,23]. However, they are only manufactured in specific dimensions and in limited aspect ratios. On the other hand, the available commercial designs are not capable of delivering the required stroke and force to our acoustic source. Flexural mechanisms are investigated in several studies to amplify the displacement of stacked piezoelectric devices. Some suggested designs that use piezoelectric devices are shown in Fig. 1. In a bridge-type mechanism that is shown in Fig. 1(a) the input and output displacements are in the same direction [24]. As seen in Fig. 1(b), a flexure hinge model uses four similar piezoelectric stack actuators

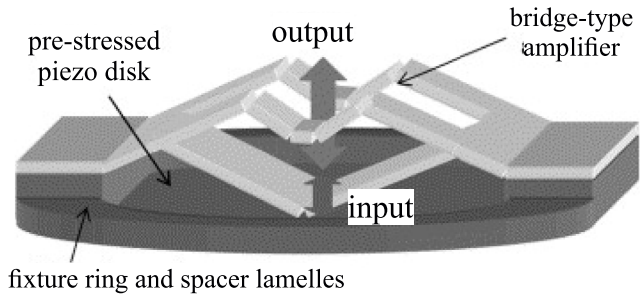

(a)

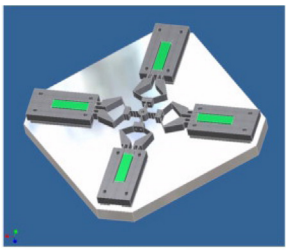

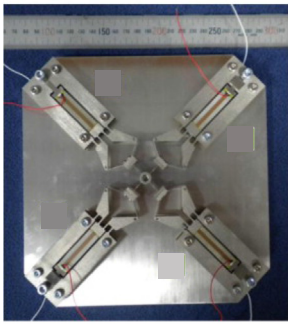

(b)

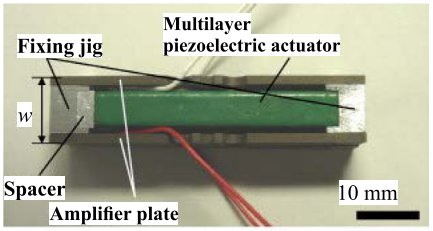

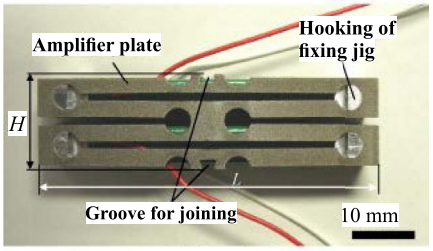

(c)

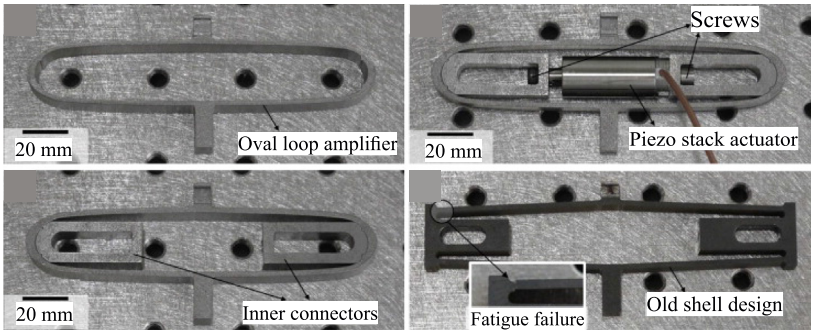

(d)

Fig. 1. Available flexural mechanism designs in literature that use piezoelectric stack actuators: (a) bridge-type [24]; (b) flexure hinge [25]; (c) honey-comb [26]; (d) ovel-shape [27].

that are located in a symmetric configuration [25]. However, the resulting displacement is in the same plane. A honey-comb flexural design (see Fig. 1(c)) can translate an input displacement into an out-of-plane displacement [26]. The suggested oval-shaped design shown in Fig. 1(d), can generate an out-of-plane output displacement [27]. However, both honeycomb and oval designs only perform at high frequencies and require high applied voltages. The available designs deliver either an in-plane

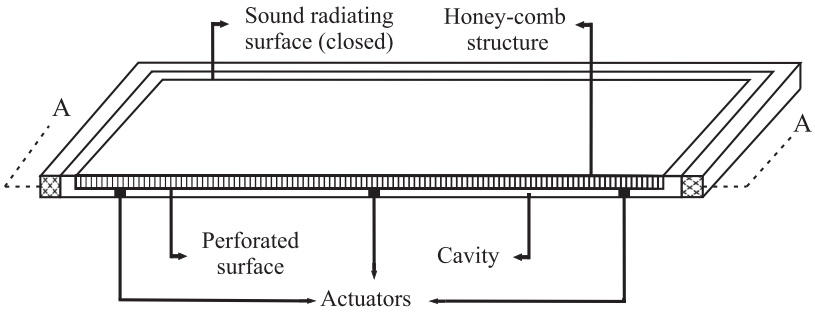

Fig. 2. A cross section view of the thin acoustic source [10].

output displacement or in the case of an out-of-plane displacement, the operating frequency range is not applicable to our thin acoustic source (frequencies below 1000 Hz are the frequencies of interest in the present work).

Limited build space of the thin acoustic source motivates the authors to investigate a new design for the actuation unit. In the current research, a thin flexural mechanism is proposed that can be used as a displacement-converter mechanism. The thin mechanism can convert the displacement of a piezoelectric stack actuator to a desired motion. A lumped model of the acoustic source is studied to obtain the required dimensions of the piezoelectric device. Based on the obtained results, a new flexural mechanism for the actuation part of the acoustic source is designed. A subsequent finite element (FE) simulation is carried out to predict the mechanical behavior of the proposed design. The fully-coupled 3D numerical model investigates the effectiveness of the proposed flexural mechanism as the excitation part of the flat acoustic source. Fluid-structural interaction is also taken into account to have an accurate prediction of the acoustical behavior of the coupled system. The lumped model of the acoustic source, which is used to obtain the optimum dimensions of the piezoelectric actuator, is also used as a first estimation to obtain the near-field sound pressure. Finally, a comparison between the numerical finite element analysis and the lumped model approach is investigated.

2. Methodology

2.1. Acoustic source

A high bending stiffness of the thin acoustic source, which is introduced in Ref. [13], is obtained by attaching the source to a sandwich structure. The thin acoustic source has a relatively small thickness and a high bending stiffness and operates in the low frequency, quasi-static regime below 1000 Hz. The structure of the acoustic source is shown in Fig. 2. It consists of a radiating surface, a honey-comb structure, a perforated surface, an air cavity, and actuators. The face of the sandwich structure internal to the source is perforated to increase the acoustic compliance. The importance of the air cavity is to reduce the required power by storing elastic energy of the air cavity. The actuation unit of the thin source receives the electric power from a connected electrical amplifier, and drives the sandwich structure. The thin acoustic source fulfills the following requirements for acoustic sources at low frequencies:

1. Due to the sufficiently large surface area of the sandwich structure, the suggested thin acoustic source has a large enclosure volume to generate sufficient acoustical power to emit sound at low frequencies,
2. Due to the small thickness, the thin acoustic source is interesting for applications with limited space,
3. Due to the existence of the sandwich structure, the resulting acoustic source is light-weight and stiff, and therefore, has a reasonably high fundamental resonance frequency for bending compared with a solid source with a similar volume,
4. Due to the existence of the perforated plate as the bottom skin of the sandwich structure, the air in the hollows of the honeycomb core adds to the air in the cavity aperture of the acoustic source. This forms a larger volume of air in the enclosure.

The details of this acoustic source are described in Refs. [10,13].

2.2. Piezoelectric actuator

Piezoelectric actuators provide the driving force to the acoustic source [10]. They are able to convert an input electric power to a mechanical power [10]. They consist of single piezoelectric layers that are typically mounted electrically in parallel and mechanically in series to achieve a larger stroke compared with the individual layers [10]. Piezoelectric actuators are energy efficient devices with minimum power loss. It is common to use either equivalent electrical circuits to model piezoelectric actu-

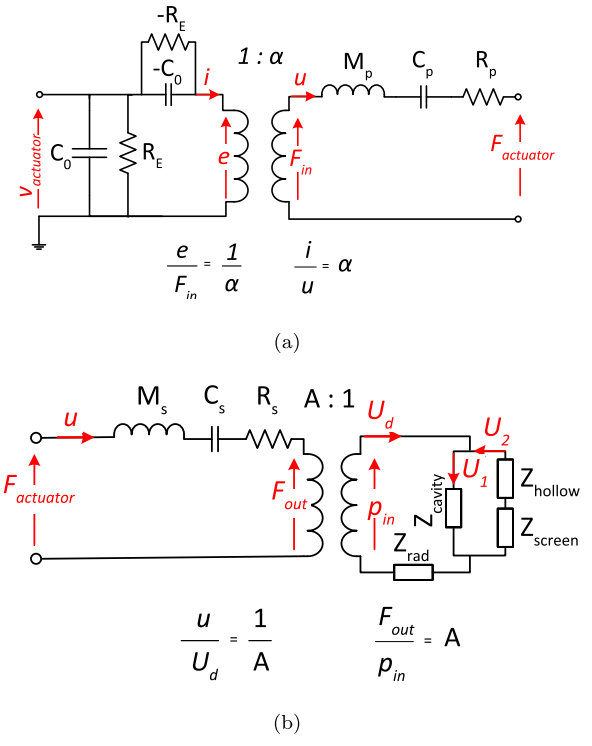

Fig. 3. The equivalent electrical circuit: (a) lumped piezoelectric stack actuator; (b) lumped acoustic source.

ators or directly solving the piezoelectric constitutive equations (see Ref. [28] for more details). In this research, an equivalent electrical circuit is used to model a lumped piezoelectric actuator.

2.3. Equivalent electrical circuit

The equivalent electrical circuit of piezoelectric stack actuators is shown in Fig. 3(a). $V_{actuator}$ shows the applied voltage to the piezoelectric element. Parameters i and e represent the output current and voltage of electrical domain, respectively. R_E is used to take the electrical loss of the piezoelectric actuator into account. Parameter α is the conversion coefficient between electrical and mechanical domains, and is calculated based on the material properties of the piezoelectric actuator. u and F_{in} show respectively the velocity and input force to the mechanical domain. C_0 shows the electrical capacitance of the piezoelectric device. M_p, C_p, and R_p are the effective mass, the compliance, and the mechanical damping of the piezoelectric actuator, respectively. According to Fig. 3(a), and using electrical analogy, the following equations can be obtained:

$$F_{in} = F_{actuator} + u(j\omega M_p + \frac{1}{j\omega C_p} + R_p), \tag{1}$$

$$e = v_{actuator} + i\frac{R_E \frac{j}{j\omega C_0}}{R_E + \frac{j}{j\omega C_0}}, \tag{2}$$

where ω is the angular frequency, and j is the imaginary unit.

An equivalent electrical circuit of a lumped model of the thin acoustic source is constructed according to the electrical analogy [14]. The resulting circuit is shown in Fig. 3(b), where u and $F_{actuator}$ are the velocity and the applied force from the actuator to the acoustic source, respectively. F_{out} is the output mechanical force of the acoustic source. The volume velocity and input pressure of the acoustic source are shown using U_d and P_{in}, respectively. M_s, C_s and R_s are respectively the mass, compliance and mechanical damping of the acoustic source. U_1 and U_2 are the volume velocities along the cavity and hollows of the honeycomb core, respectively. The conversion coefficient, A, is the surface area of the acoustic source. Parameters Z_{cavity}, Z_{hollow}, Z_{screen} and Z_{rad} represent the equivalent acoustical impedance of the air in the cavity, the air in the hollows of the honeycomb structure, the perforated plate, and the radiation impedance of the acoustic source. The acoustical impedances of the air in the cavity and air in the hollows of the honeycomb core are defined as follows:

$$Z_{cavity} = \frac{v_{cavity}}{\rho_0 c_0^2}, \tag{3}$$

Fig. 4. The equivalent radiation impedance of the thin acoustic source using an electrical circuit in series [30].

$$Z_{hollows} = \frac{v_{h.c}}{\rho_0 c_0^2}, \tag{4}$$

in which the parameters v_{cavity} and $v_{h.c}$ are the volume of air in the cavity and in the hollows of the honeycomb structure, respectively, and ρ_0 and c_0 are respectively the density and speed of sound in the air. The acoustical impedance of the perforated panel is evaluated as:

$$Z_{screen} = \frac{\rho_0 c_0 \zeta_{screen}}{A}, \tag{5}$$

where ζ_{screen} can be obtained using the following equation (see Ref. [14] for details):

$$\zeta_{screen} = \frac{2}{\sigma}\sqrt{\frac{2\mu k}{\rho_0 c_0}}\left(\frac{t_p}{d_h} + 1 - \sigma\right) + j\frac{k}{\sigma}\left(t_p + 0.85 d_h(1 - \sqrt{\frac{\sigma}{\pi}})\right). \tag{6}$$

According to this equation, ζ_{screen} is a function of the thickness of the perforated plate, t_p, and the distance between any two neighboring holes, d_h. One can obtain the radiation impedance, Z_{rad} (see Fig. 3(b)) considering the radiation impedance of a circular rigid piston radiator which is mounted in an infinite baffle, and has the same surface area as the rectangular acoustic source [29]. Therefore, Z_{rad} can be obtained using the resulting equation from the Helmholtz integral [29]:

$$Z_{rad} = \frac{\rho_0 c_0}{A}(R_{rad} + j\omega M_{rad}), \tag{7}$$

$$R_{rad} = 1 - \frac{2J_1(2ka)}{2ka},$$

$$M_{rad} = \frac{1}{\omega}\frac{2K_1(2ka)}{2ka}. \tag{8}$$

where a is the radius of the equivalent circular piston, k is the wave number, and J_1 and K_1 are Bessel and Struve functions of the first kind, respectively. This expression can be described using an equivalent electrical circuit shown in Fig. 4 [30]. Acoustical mass, M_{rad}, and resistance, R_{rad}, are arranged as the electrical elements in series in the equivalent circuit [30]. Using the electrical analogy, the following equation can be concluded from the electrical circuit of the lumped acoustic source in Fig. 3(b):

$$F_{actuator} = u(j\omega M_s + \frac{1}{j\omega C_s} + R_s) + A^2 u\left(\frac{Z_{cavity}(Z_{hollow} + Z_{screen})}{Z_{cavity} + Z_{hollow} + Z_{screen}}\right) + A^2 u Z_{rad}. \tag{9}$$

$F_{actuator}$ and u in Eqs. (1) and (2) can be substituted in Eq. (9), and subsequently, the fully-lumped model can be solved using the electrical analogy.

As mentioned in Sec. 1, the main objective in the present work is to design the actuation unit of the thin acoustic source in such a way that it contributes to the maximum radiation power of the complete acoustic source system. Therefore, using the electrical analogy in Fig. 3, the radiation power of the complete lumped acoustic source is defined as the power that is generated in the component Z_{rad}. This power generation occurs when U_d passes through the radiation impedance, Z_{rad}, in the circuit. P_{rad} can be evaluated using the following equation:

$$P_{rad} = 0.5\Re(U_d^2 Z_{rad}^*), \tag{10}$$

where Z_{rad}^* is the complex conjugate of the radiation impedance. Since the current in the acoustical domain, U_d, is a function of all the electrical elements in the circuit, the resulting radiation power is also a function of those elements. Therefore, P_{rad} is a function of i_{piezo} and V_{piezo}. That implies that P_{rad} is a function of the characteristics of the piezoelectric device, i.e. the dimensions of the piezoelectric device. Considering Eq. (10) and the relation between P_{rad} and the dimensions of the piezoelectric actuator, an optimization study can determine the optimum size of the actuator that results in a maximum radiation power of the thin acoustic source.

2.4. Optimization

The equivalent lumped electrical circuit of the thin acoustic source is used in combination with MATLAB R2015b version 8.6 optimization toolbox [31]. Due to having a nonlinear objective function, the Sequential Quadratic Programming algorithm [32]

Table 1
Material properties of the piezoelectric stack actuator that is used in the optimization study [33].

Parameters	Symbol	Value	SI unit
Material	–	PSt150	–
Charge coefficient	d_{33}	640	10^{-12} C.N^{-1}
Relative permittivity	$\frac{\epsilon^T}{\epsilon_0}$	5400	–
Elastic compliance	s^E	18.1	10^{-12} m^2 N^{-1}
Density	ρ_{piezo}	8000	kg.m^{-3}
Dielectric loss factor	$\tan\delta$	200×10^{-4}	–
Mechanical quality factor	Q_m	70	–

(SQP) is employed. Solving the optimization problem, the optimum dimensions of the required piezoelectric stack actuator are obtained. The following optimization problem is defined:

$$\begin{aligned} &\underset{r_p, l_p}{\text{maximize}} \quad P_{rad}(r_p, l_p) \\ &\text{subject to} \quad m_{piezo} = \text{constant}, \end{aligned} \tag{11}$$

where r_p and l_p are the radius and the length of the piezoelectric stack actuator, respectively. According to Eq. (11), the only constraint is the mass of the piezoelectric stack actuator, which is a linear function of the dimensions of the actuator. The mass of the piezoelectric stack actuator is considered to be equal to the mass of the voice coil actuator that was used in a previous study in Ref. [14] in the design of the same acoustic source ($m_{\text{piezo}} = 43.7$g). The objective is maximizing the radiation power (P_{rad}) of the acoustic source at a low frequency below 1000 Hz, when it is excited by a piezoelectric stack actuator with a constant mass. The radiation power in Eq. (11) is calculated according to the electrical analogy, and can be determined using Eq. (10). According to Eq. (10) and the electrical analogy (see Fig. 3), the objective function in the optimization problem is a function of the current in the acoustical domain, U_d. The current in the acoustical domain is a function of the impedance of all the components in the equivalent electrical circuit, including the electrical capacitance of the piezoelectric actuator. The electrical capacitance of the actuator, C_0, is a function of the dimensions of the actuator, r_p and l_p. Therefore, according to the electrical analogy, the relation between the objective function is a nonlinear complex function (see Ref. [10] for more details). The material properties of the piezoelectric stack actuator that is used in the optimization study is listed in Table 1. Therefore, the optimization problem is solved for a specific piezoelectric material, where the only design variables are the dimensions of the actuator. Note that both mass and density of the piezoelectric stack actuator are defined as constant parameters. Hence, the volume of the optimum actuator is constant. It can be concluded that the design variables (r_p and l_p) are dependent. Therefore, the study can be simplified as a single-variable optimization problem with the defined upper and lower bounds for the radius and the length of the optimum actuator. The defined upper and lower bounds for the dimensions of the optimum actuators ensure that the aspect ratio between the radius and the length of the actuator remains within an allowable range. In the present study, the optimization problem is solved for the optimum radius of the actuator, which has to be in the range of 3 mm $< r_p <$ 5 mm, and the length of the actuator is considered to be in the range of 20 mm $< l_p <$ 100 mm.

The result of optimization is shown in Fig. 5. According to the figure, the maximum radiation power of the acoustic source corresponds to the optimum radius of 4 mm. This radius corresponds to the length of 100 mm for the piezoelectric stack actuator (which is equal to the upper bound length in solving the optimization problem). Due to the constant volume of the optimum piezoelectric stack actuator, the longer the length of the actuator, the smaller the radius.

The introduced upper and lower bounds result in an optimum actuator with an aspect ratio that is the closest to unity. The maximum radiation impedance is obtained at frequencies below 1000 Hz. The optimum value of the radiation impedance in the figure is evaluated at 100 Hz.

2.5. Requirements and limitations

According to the outcome of the optimization, a piezoelectric stack actuator with a length of 100 mm is needed. This optimum l_p is obtained for the specific piezoelectric material with the defined mass and density of the actuator (see Table 1). The length and the radius of the optimum actuator are chosen in such a way that the aspect ratio remains close to unity. However, the available space for the actuator in the structure of the thin acoustic source is limited to the cavity gap with the thickness of only 10 mm. Since the optimum piezoelectric element with $l_p = 100$ mm is not fitted in the available gap, the use of a displacement-converter mechanism is crucial. With the aid of a displacement-converter mechanism, the optimum actuator can be used while it is mounted in the horizontal plane. Therefore, the displacement of the piezoelectric device in a direction without any space constraint (in the horizontal plane) can be converted to the desired vertical displacement (in the out-of-plane z-axis direction).

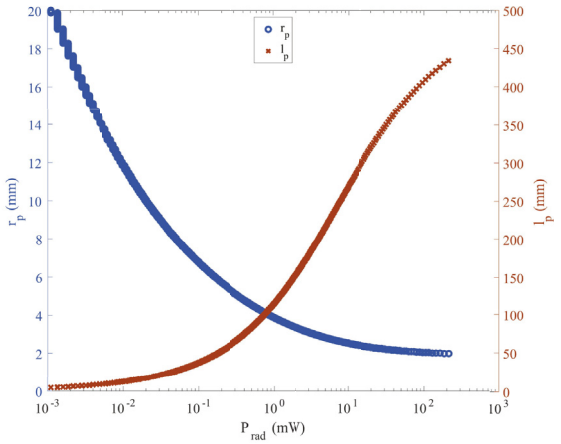

Fig. 5. The result of the optimization study that shows the optimum radius and length of the piezoelectric stack actuator to achieve maximum radiation power of the thin acoustic source.

3. Numerical modeling

3.1. Flexures, the actuation part of the acoustic source

Using a flexural displacement-converter mechanism, it is possible to use piezoelectric devices in a horizontal *xy*-plane and obtain the converted out-of-plane displacement in the direction of the *z*-axis. In the present paper, a 3D numerical finite element simulation in COMSOL Multiphysics 5.3a software package is performed [34]. The designed mechanism has only one degree of freedom for the displacement in the vertical direction (in the direction of the *z*-axis).

The schematic of the suggested flexural mechanism is shown in Fig. 6(a). As seen in this figure, a single piezoelectric stack actuator is used to provide the driving force to the flexural mechanism. The flexural mechanism is made of a single piece, and has two fixed boundaries. Two ends of the piezoelectric device are attached to the flexural design. Using flexural notch hinges at the two ends of the piezoelectric device ensures that only axial loads are applied to the piezoelectric device. Both ends of the flexural mechanism are fixed to resemble fixed joints. The horizontal deformation of the piezoelectric stack actuator in the direction of the *x*-axis is translated to the output motion in the direction of the *z*-axis (see Fig. 6(b)). Due to the symmetric design, the central part of the mechanism only experiences a vertical displacement. The dimension of the designed mechanism in the direction of the *z*-axis is only 10 mm. Therefore, it can be fitted in the air cavity of the thin acoustic source. The out-of-plane dimension of the flexural mechanism in the direction of the *y*-axis is 20 mm to ensure that the mechanism is stiff enough in that direction.

3.2. Coupled model of the flexural design and the thin acoustic source

A 3D finite element model (FEM) of the thin acoustic source is used to analyze the suggested flexural mechanism. The numerical study in COMSOL Multiphysics predicts the near-field sound pressure that is radiated from the flat acoustic source. A piezoelectric stack actuator is modeled numerically according to the special electrical and mechanical interfaces available in the software. A voltage of 150 V is applied to the piezoelectric element. The fully-coupled finite element problem is solved by considering the electrical, mechanical and acoustical interfaces. Fig. 7 shows the first bending mode of the sandwich plate in the fully-coupled model. The fully-coupled finite element model takes into account the fluid-structural interaction. The fully-coupled model considers identical normal velocities for both the radiating plate of the acoustic source, $v_{n,Structure}$, and the near-field air particles on the surface, $v_{n,Fluid}$:

$$v_{n,Structure} = v_{n,Fluid}. \tag{12}$$

Moreover, the applied normal force from the sandwich plate to the acoustical domain, $F_{n,Structure}$, has the same value but an opposite direction as the force applied from the acoustical domain to the radiating plate, $F_{n,Fluid}$:

$$F_{n,Structure} = -F_{n,Fluid}. \tag{13}$$

As a result of the finite element analysis, the generated sound by the radiating surface of the acoustic source is calculated and is shown in Fig. 8. As seen in this figure, the near-field sound pressure level of the thin acoustic source is predicted by the finite element model at 50 Hz, 200 Hz, and at resonance (436 Hz). The acoustic source can reach 70 dB, 95 dB and 120 dB at 50 Hz, 200 Hz, and at resonance, respectively. According to the Equal-loudness-level contours [35], the obtained sound pressure

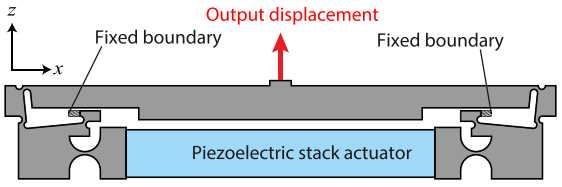

(a)

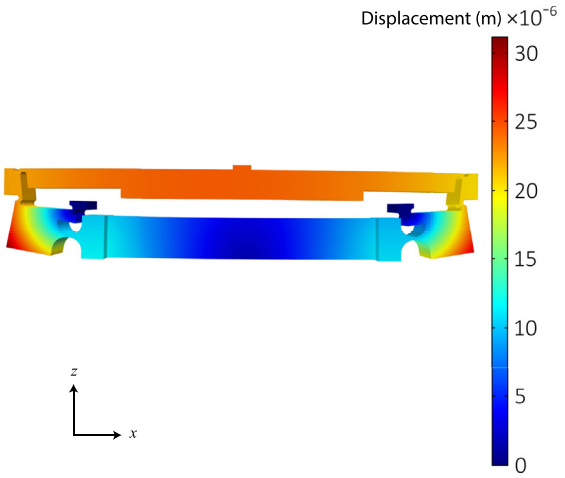

(b)

Fig. 6. The suggested displacement-converter mechanism: (a) the schematic of the proposed mechanism; (b) the deformed mechanism during operation.

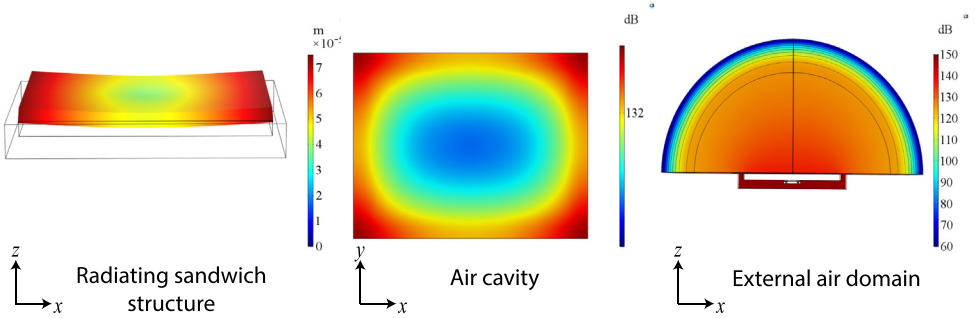

Fig. 7. The mechanical and acoustical mode shapes of the fully-coupled acoustic source system that are obtained at the first resonance frequency (bending mode at 436 Hz).

values are within the audible range. The reference sound pressure of 20×10^{-6} Pa is considered in the simulation for obtaining the sound pressure level in the near-field and far-field calculations.

4. Results and discussions

A fully-coupled 3D finite element analysis in COMSOL Multiphysics predicts the acoustical behavior of the thin acoustic source that is actuated by the proposed flexural mechanism. Fig. 9 shows that the proposed flexural mechanism is useful in the structure of the thin acoustic source. This is due to the successful conversion of the in-plane input motion into a perpendicular out-of-plane motion that has a relatively similar magnitude as the input. According to the finite element analysis, a rigid-body motion of the actuation part of the thin acoustic source is achieved below 200 Hz (see Fig. 9). The rigid-body motion of the source ensures a flat frequency response in the low frequency range. Fig. 9 shows a comparison between the input and output motions of the suggested flexural mechanism. Below the first resonance of the coupled system (at 436 Hz), the horizontal displacement of

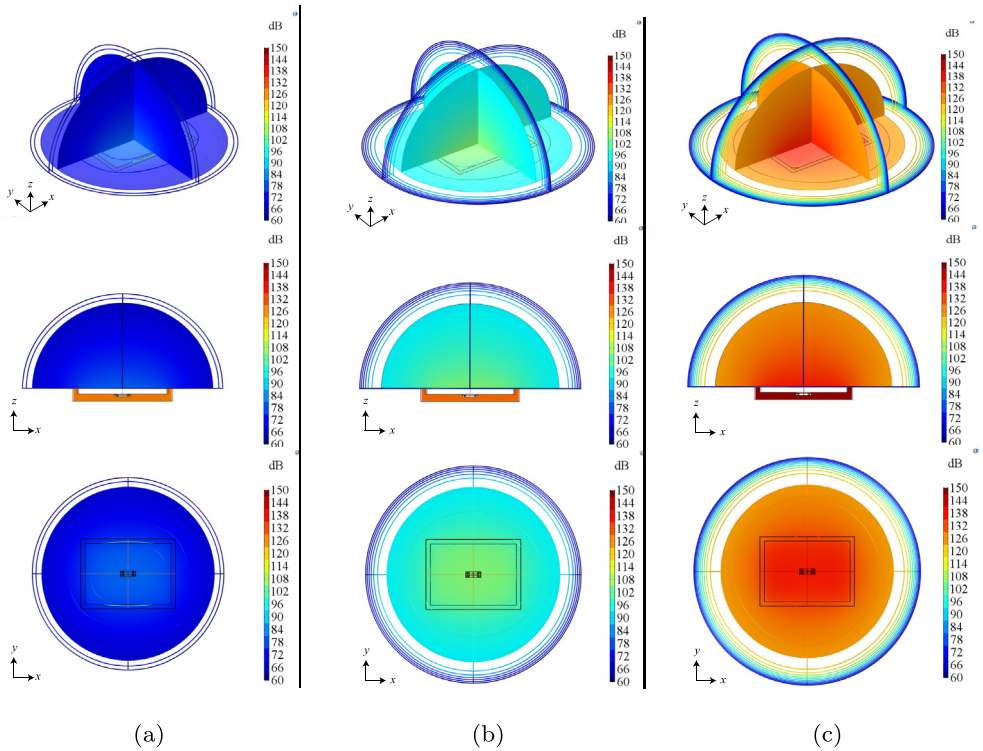

Fig. 8. Sound pressure level of the air in the cavity, the near-field air, and the far-field air of the thin acoustic source; the results are evaluated using a reference pressure of 20×10^{-6} Pa at various frequencies: (a) 50 Hz; (b) 200 Hz; (c) 436 Hz.

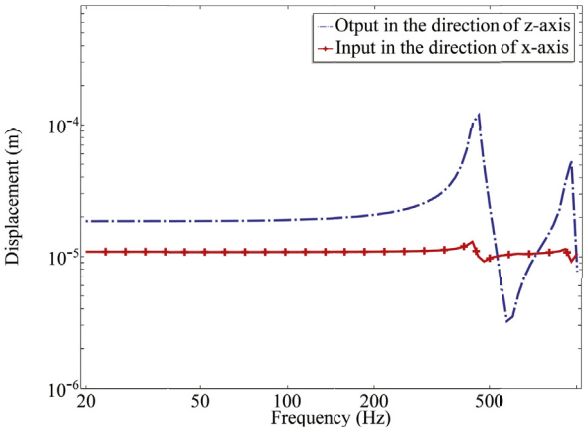

Fig. 9. A comparison between the input and output displacements of the proposed motion-converter mechanism; the results are obtained from the FE analysis over the operating frequency range below 1000 Hz.

the piezoelectric actuator in the direction of the x-axis is approximately 1.2×10^{-5} m. In the same frequency range, the output displacement of the actuation mechanism in the direction of the z-axis is 1.8×10^{-5} m. One can determine the amplification ratio of the flexural mechanism as the ratio between the output and input motions to be 1.5. Fig. 10 shows the relation between the input and output motions of the proposed motion-converter mechanism. The relation between the input and output motions in the figure is linear. This linear relation ensures that the proposed motion-converter mechanism is a linear system.

The acoustical behavior of the thin acoustic source that is actuated by the suggested flexural mechanism is shown in Fig. 11. The sound pressure level on a point that is located in the center of the radiating plate is investigated in the figure. The first resonance of the coupled system occurs at 436 Hz. This first resonance corresponds to the first bending mode of the sandwich source. As seen in the figure, above 30 Hz, the sound pressure level on the surface of the acoustic source is within the audible

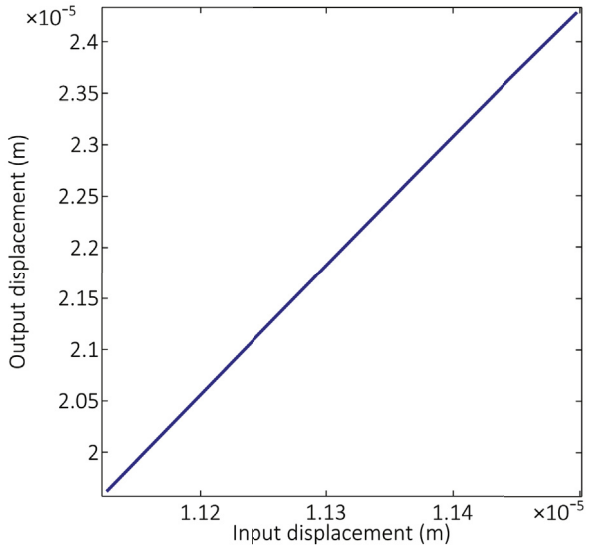

Fig. 10. The linear relation between the input and output motions of the proposed motion-converter mechanism that is obtained from the FE analysis.

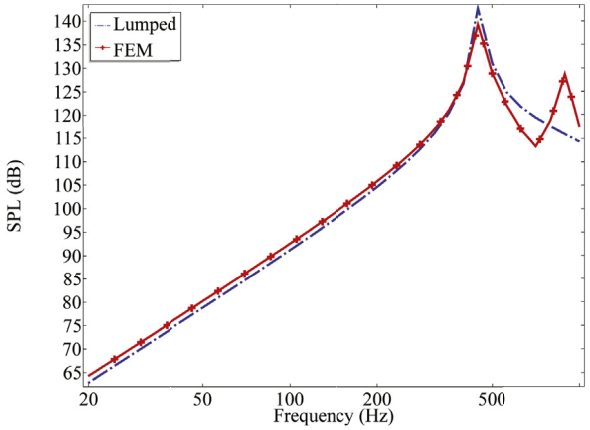

Fig. 11. A comparison between the obtained sound pressure level at a point in the center of the radiating surface of the thin acoustic source; the results are obtained using both the fully-FEM model and the lumped model (the reference sound pressure is equal to 20×10^{-6}Pa).

range (according to the Equal-loudness-level contours [35]). The figure shows a good agreement between the FEM and the lumped model of the thin acoustic source, especially, below the first bending mode of the thin sandwich structure at 436 Hz. Therefore, the result of the lumped model in the figure can be used to validate the FEM analysis, especially below the first resonance of the coupled acoustic source system. It can be concluded from the figure that below the first resonance, using the lumped model is sufficient and computationally less expensive to obtain the SPL of the acoustic source than using the finite element model.

The relation between the applied voltage to the piezoelectric stack actuator and the generated sound pressure level of the thin acoustic source is shown in Fig. 12. The applied DC voltage to the actuator is 75 V, and the peak value of the applied AC voltage varies from 5 V to 75 V. The SPL is obtained on a point that is located in the middle of the vibrating surface of the thin acoustic source. As seen in the figure, increasing the applied AC voltage to the piezoelectric stack actuator results in an increase in the generated sound pressure level of the thin acoustic source. The figure is obtained at 100 Hz.

The directivity of the thin acoustic source is shown in Fig. 13. As seen in the figure, the directivity of the generated sound pressure level is dependent on the operating frequency. The directivity pattern in the figure is normalized with respect to the angle 0°. The associated sound pressure level at various frequencies in half space is shown in the figure. The angle 0° corresponds to the normal line to the vibrating surface of the thin acoustic source, which is in the direction of the z-axis (see Fig. 8). As seen in the figure, the radiation pattern, especially, along the normal line with the angle 0°, has a relatively similar pattern for the frequencies below 550 Hz. Fig. 14 shows an overview of the far-field directivity pattern in the xz-plane. With the angle

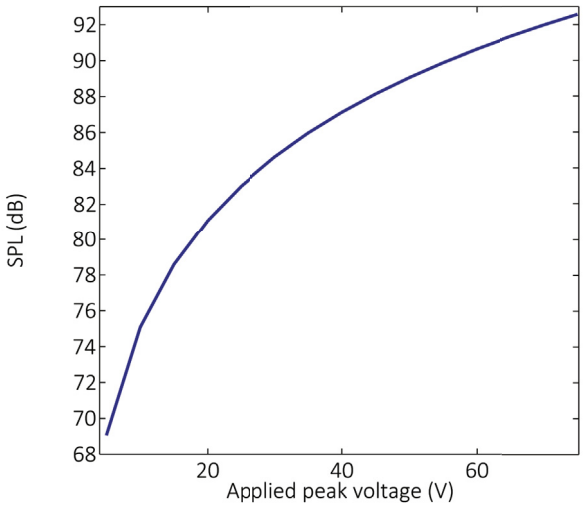

Fig. 12. The relation between the peak value of the input AC voltage to the piezoelectric stack actuator and the output sound pressure level of the proposed motion-converter mechanism (the reference sound pressure is equal to 20×10^{-6}Pa).

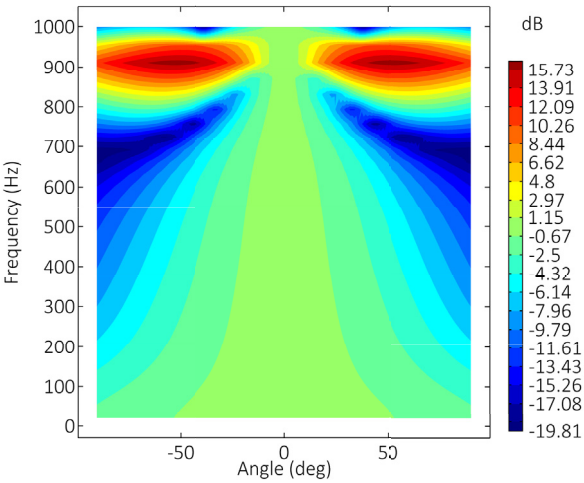

Fig. 13. The normalized far-field directivity of the generated sound pressure level of the thin acoustic source (the angle 0° corresponds to the normal line to the vibrating surface in the positive direction of the *z*-axis).

0° pointing at the direction of the *z*-axis, the polar directivity plot is shown for multiple frequencies. The figure is obtained for various distance ranges from the vibrating surface of the thin acoustic source in the far-field. As seen in the figure, the directivity of the thin acoustic source is dependent on the studied frequencies.

As seen in the figure, the directivity pattern of the thin acoustic source has the biggest beam lobe in the direction of angle 0°, especially below the fundamental resonance of the coupled acoustic source system (436 Hz). According to the figure, below the fundamental resonance frequency, the directivity pattern is a single-lobe beam pointing at angle 0°.

5. Summary

In the present research, the optimization study shows that the required length for the piezoelectric stack device as the excitation part of a thin acoustic source is approximately 100 mm. However, due to limited build space, it is not possible to use a piezoelectric stack actuator with a length larger than 10 mm. Therefore, a flexural mechanism is designed to be used as a displacement-converter mechanism. The flexural mechanism is simulated numerically using COMSOL Multiphysics software package. The acoustical behavior of the thin acoustic source is numerically investigated when the proposed mechanism is used as the actuation part. The suggested flexural motion-converter mechanism makes it possible to use a thin piezoelectric actuator.

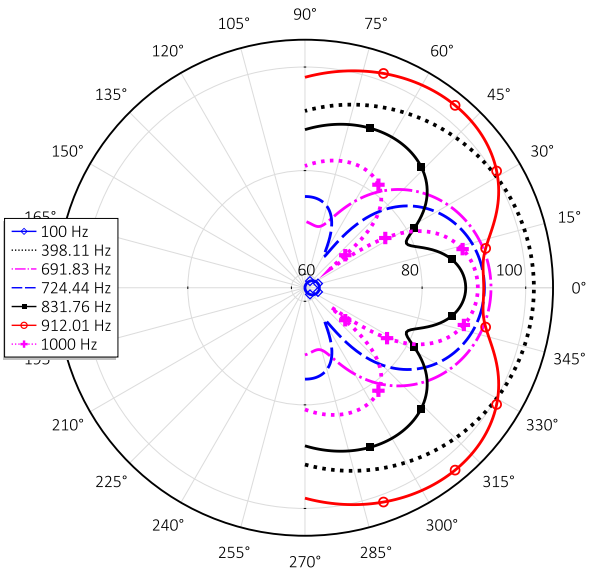

Fig. 14. The polar far-field directivity pattern of the thin acoustic source at multiple frequencies when the reference angle of 0° corresponds to the positive direction of the *z*-axis in the *xz*-plane.

The proposed thin actuation design can successfully convert a motion of the piezoelectric stack actuator in the direction of the *x*-axis to an out-of-plane motion in the direction of the *z*-axis. A lumped model of the thin acoustic source is compared with the results of a 3D numerical finite element simulation. The obtained sound pressure level on the surface of the sandwich plate of the source is identical in both the numerical FEM and the lumped models. A comparison between the SPL obtained from both the lumped model and the numerical FE analysis shows that the numerical model can successfully predict the behavior of the acoustic source and the proposed actuation unit up to the fundamental resonance of the acoustic source system. The directivity of the generated sound pressure of the thin acoustic source is obtained in the far-field space to investigate the frequency-dependency of the directivity.

Acknowledgements

The authors gratefully acknowledge the European Commission for its support of the Marie Skłodowska Curie program through the ITN ANTARES project (GA 606817).

References

[1] M. Colloms, High-performance Loudspeakers, Wiley, 2005, https://www.amazon.com/High-Performance-Loudspeakers-Martin-Colloms/dp/0470094303.
[2] B. Petitjean, I. Legrain, F. Simon, S. Pauzin, Active control experiments for acoustic radiation reduction of a sandwich panel: feedback and feedforward investigations, J. Sound Vib. 252 (1) (2002) 19–36, https://doi.org/10.1006/jsvi.2001.4022.
[3] Y. Luo, S. Xie, X. Zhang, The actuated performance of multi-layer piezoelectric actuator in active vibration control of honeycomb sandwich panel, J. Sound Vib. 317 (3) (2008) 496–513, https://doi.org/10.1016/j.jsv.2008.03.047.
[4] T. Lok, Q. Cheng, Free vibration of clamped orthotropic sandwich panel, J. Sound Vib. 229 (2) (2000) 311–327, https://doi.org/10.1006/jsvi.1999.2485.
[5] T. Lok, Q. Cheng, Free and forced vibration of simply supported, orthotropic sandwich panel, Comput. Struct. 79 (3) (2001) 301–312, https://doi.org/10.1016/S0045-7949(00)00136-X.
[6] E. Nilsson, A. Nilsson, Prediction and measurement of some dynamic properties of sandwich structures with honeycomb and foam cores, J. Sound Vib. 251 (3) (2002) 409–430, https://doi.org/10.1006/jsvi.2001.4007.
[7] M. Vivolo, B. Poluymers, D. Vandepitte, W. Desmet, An experimental-numerical study on the vibro-acoustic characterization of honeycomb lightweight panels, in: Proceedings of the International Conference on Noise and Vibration Engineering ISMA 2010, Leuven, Belgium, 2010, pp. 2197–2211. http://past.isma-isaac.be/downloads/isma2010/papers/isma2010_0486.pdf.
[8] A. Putra, D. Thompson, Sound radiation from perforated plates, J. Sound Vib. 329 (20) (2010) 4227–4250, https://doi.org/10.1016/j.jsv.2010.04.020.
[9] A. Putra, D. Thompson, Radiation efficiency of unbaffled and perforated plates near a rigid reflecting surface, J. Sound Vib. 330 (22) (2011) 5443–5459, https://doi.org/10.1016/j.jsv.2011.05.033.
[10] F. Tajdari, A.P. Berkhoff, A. de Boer, Numerical modeling of electrical-mechanical-acoustical behavior of a lumped acoustic source driven by a piezoelectric stack actuator, in: P.P. Sas (Ed.), Proceedings ISMA 2016, KULeuven, 2016, pp. 1261–1275.
[11] S. Elliott, P. Nelson, Active noise control, IEEE Signal Process. Mag. 10 (4) (1993) 12–35, https://doi.org/10.1109/79.248551, https://ieeexplore.ieee.org/document/248551.
[12] L. Beranek, T. Mello, Acoustics: Sound Fields and Transducers, Academic Press, 2012, https://doi.org/10.1016/C2011-0-05897-0, https://www.sciencedirect.com/book/9780123914217/acoustics-sound-fields-and-transducers.
[13] A. P. Berkhoff, Sound generator, US Patent, US20 100 111 351 A2 (2010).
[14] J. Ho, A.P. Berkhoff, Flat acoustic sources with frequency response correction based on feedback and feed-forward distributed control, J. Acoust. Soc. Am. 137 (4) (2015) 2080–2088, https://doi.org/10.1121/1.4914997.

[15] J. Ho, Control Source Development for Reduction of Noise Transmitted through a Double Panel Structure, Ph.D. thesis, University of Twente, Enschede, The Netherlands, Jully 2014.
[16] F. Grondin, F. Michaud, Lightweight and optimized sound source localization and tracking methods for open and closed microphone array configurations, Robot. Autonom. Syst. 113 (2019) 63–80, https://doi.org/10.1016/j.robot.2019.01.002.
[17] T. Padois, O. Doutres, F. Sgard, A. Berry, Optimization of a spherical microphone array geometry for localizing acoustic sources using the generalized cross-correlation technique, Mech. Syst. Signal Process. 132 (2019) 546–559, https://doi.org/10.1016/j.ymssp.2019.07.010.
[18] D.B. Ward, E.A. Lehmann, R.C. Williamson, Particle filtering algorithms for tracking an acoustic source in a reverberant environment, IEEE Trans. Speech Audio Process. 11 (6) (2003) 826–836, https://doi.org/10.1109/TSA.2003.818112.
[19] J. Loncaric, S.V. Tsynkov, Optimization of acoustic source strength in the problems of active noise control, SIAM J. Appl. Math. 63 (4) (2003) 1141–1183, https://doi.org/10.1137/S0036139902404220.
[20] S.T. Smith, Flexures, Elements of Elastic Mechanisms, CRC Press, University of North Carolina, USA, 2000.
[21] H. Soemers, Design Principles for Precision Mechanisms, T-Pointprint, University of Twente, The Netherlands, 2011.
[22] F. Claeyssen, R. Le Letty, F. Barillot, O. Sosnicki, Amplified piezoelectric actuators: static & dynamic applications, Ferroelectrics 351 (1) (2007) 3–14, https://doi.org/10.1080/00150190701351865.
[23] R. Lucinskis, C. Mangeot, Dynamic Characterization of an Amplified Piezoelectric Actuator, 2016.
[24] J. Juuti, K. Kords, R. Lonnakko, V.-P. Moilanen, S. Leppvuori, Mechanically amplified large displacement piezoelectric actuators, Sensor Actuator A Phys. 120 (1) (2005) 225–231, https://doi.org/10.1016/j.sna.2004.11.016.
[25] J. Guo, S.K. Chee, T. Yano, T. Higuchi, Micro-vibration stage using piezo actuators, Sensor Actuator A Phys. 194 (2013) 119–127, https://doi.org/10.1016/j.sna.2013.01.025.
[26] M. Muraoka, S. Sanada, Displacement amplifier for piezoelectric actuator based on honeycomb link mechanism, Sensor Actuator A Phys. 157 (1) (2010) 84–90, https://doi.org/10.1016/j.sna.2009.10.024.
[27] T. Yeom, T.W. Simon, M. Zhang, M.T. North, T. Cui, High frequency, large displacement, and low power consumption piezoelectric translational actuator based on an oval loop shell, Sensor Actuator A Phys. 176 (2012) 99–109, https://doi.org/10.1016/j.sna.2012.01.001.
[28] IEEE, IEEE Standard on Piezoelectricity, 1987https://doi.org/10.1109/IEEESTD.1988.79638.
[29] A. Pierce, Acoustics, an Introduction to its Physical Principles and Applications, The Acoustical Society of America, New York, USA, 1989.
[30] in: Proceedings 25th International Congress on Sound and Vibration 2018, ICSV25.
[31] MATLAB R2015b documentations. https://nl.mathworks.com/help/.
[32] J.S. Arora, Introduction to Optimum Design, Academic Press, 2017, https://doi.org/10.1016/C2013-0-15344-5, https://www.elsevier.com/books/introduction-to-optimum-design/arora/978-0-12-800806-5.
[33] Specifications, PSt150, piezomechanik. https://www.piezomechanik.com/fileadmin/filestorage/Kataloge/en/Piezomechanik_Product_range_Low_2017_WEB.pdf, (Accessed 16 May 2019).
[34] COMSOL Multiphysics 5.3a documentations. https://www.comsol.com/documentation.
[35] H. Fletcher, W.A. Munson, Loudness, its definition, measurement and calculation, J. Acoust. Soc. Am. 5 (1933) 82–108, https://doi.org/10.1121/1.1915633.